Flaking of black anodic films in space environment: Ageing and numerical simulation

Yann Goueffon, Grégory Aldebert, Catherine Mabru, Laurent Arurault, Claire Tonon, Pascale Guigue

Flaking of black anodic films in space environment: Ageing and numerical simulation

Yann Goueffon [a], Grégory Aldebert [b], Catherine Mabru [b,*], Laurent Arurault [c], Claire Tonon [a], Pascale Guigue [d]

[a] EADS ASTRIUM Satellites, 31 Avenue des Cosmonautes, 31402 Toulouse Cedex 4, France
[b] Université de Toulouse, ISAE, Institut Clément Ader, 10 Avenue Edouard Belin, BP 54032, 31055 Toulouse Cedex 4, France
[c] Université de Toulouse, CIRIMAT, UPS/INPT/CNRS, LCMIE, Bat 2R1, 118 Route de Narbonne, 31062 Toulouse Cedex 9, France
[d] CNES, 18 Avenue Edouard Belin, 31401 Toulouse Cedex 9, France

Keywords:
Flaking
Crack propagation
Numerical simulation
Crazing
Thermal ageing
Black anodic film

A B S T R A C T

Black coatings can be used for managing passive thermal control on spacecraft and for avoiding stray light in optical equipment. Inorganic black anodizing of aluminium alloys is a solution to obtain films with a low outgassing and a sufficient thermal stability for this kind of application. Flaking of these coatings has sometimes been observed after thermal cycling on 2XXX and 7XXX aluminium alloys. This phenomenon could generate particulate contamination on satellites optics and may affect mission lifetime. In this work, the influence of thermal cycling on the adhesion of the films was investigated thanks to both a qualitative method (peel-test) and a quantitative method (scratch-test). It has been shown that differential dilatations and dehydration of the film result in stresses inside the film. A finite element model was developed to identify the mechanisms of crack propagation and bifurcation inside the film and thus explain the reasons of flaking. Especially, it has been shown that cracks can bifurcate and propagate in the film along the interface under thermal solicitation resulting in a mixed opening/shearing mode loading at the crack tip.

1. Introduction

Under space vacuum, thermal exchanges between a satellite and its environment are only radiative. The spacecraft temperature is mainly depending on the interactions with three main external sources (the Earth, the sun and the deep cold space). The Earth is emitting an infrared flux heating the satellite while, on the contrary, the deep cold space is equivalent to a source at 3 K and allows evacuation of heat. Those two heat fluxes can be considered as approximately constant during revolutions of the satellite. Nevertheless, the main heating source is the sun (direct and albedo fluxes). Successive passages in the shadow of the Earth result in thousands thermal cycles suffered by the satellite during its lifetime. The temperature of exposed parts like solar arrays can typically vary between −140 and +140 °C.

The radiative exchanges of a part are driven by its thermo-optical properties (ε emissivity and α_s solar absorptance) and the equilibrium temperature is directly linked to the ratio α_s/ε (Agrawal, 1986). The required specification directly depends on the equipment needs. Cold parts can be obtained for $\alpha_s/\varepsilon < 1$ (Siva Kumar et al., 1999) while a ratio $\alpha_s/\varepsilon > 1$ results in a high equilibrium temperature (Saxena et al., 2006).

Warm parts are obtained for a ratio close to one. In the case of aluminium alloys, largely used in spacecraft design, different surface treatments are available to provide such thermo-optical properties: black paints (McCroskey et al., 2000), micro-arc oxidation (Shrestha et al., 2006; Wu et al., 2007), electro-deposition (Magdy and Ibrahim,

* Corresponding author. Tel.: +33 561 339 150; fax: +33 561 339 095.
E-mail address: Catherine.mabru@isae.fr (C. Mabru).

2006) or black anodizing (Goueffon et al., 2009a; LeVesque et al., 1992; Shashikala et al., 2006).

The black inorganic anodizing of aluminium alloys is used to provide specific thermo-optical properties to surfaces and then manage passive thermal control. Actually, the process allows the increase of the normal emissivity to 0.90 and the solar absorptance to 0.93 (ECSS-Q-ST-70-03C, 2008). In addition, the high absorptance avoids stray lights reflections that could be harmful especially near optical instruments while the use of inorganic dyes limits the outgassing in vacuum. Nevertheless cases of flaking of black anodic films were sometimes observed on aluminium from 2XXX and 7XXX series after thermal cycling performed to simulate the space environment (ESA Alert, 2005; Goueffon et al., 2009a). Such particles could pollute sensitive equipment of the satellite and shorten the lifetime of the mission.

The aim of this work is to study the environmental conditions leading to flaking of the anodic film. The influence of ageing on the adhesion of the film was measured thanks to three different methods: the peel test, the scratch test and four-point bending test. Flaking was then reproduced after experimental thermal cycling and numerical simulation was used to understand the mechanisms involved.

2. Experimental procedure

The aluminium substrate was AA 7175 T7351 often used in the space industry. Some cases of flaking have been observed on this alloy. Two sizes of samples were used: $40 \times 20 \times 3$ mm for scratch and peel tests and $160 \times 20 \times 10$ mm for bending tests.

2.1. Process of black anodizing

The black anodizing process followed the ESA standard (ECSS-Q-ST-70-03C, 2008) for spacecraft design. It consists in four main steps: pretreatments, anodizing, inorganic colouring and sealing.

The aluminium sheets were degreased with ethanol, etched in an aqueous mixed solution of Na_2CO_3/Na_3PO_4 for 5 min at 93 °C and neutralised 3 min at room temperature in HNO_3 (50% v/v). The samples were rinsed with distiled water at the end of each step.

The anodizing was performed in sulphuric acid during 60 min with a current density of 1.25 A/dm^2. It results in the growth of a porous oxide film with a typical thickness of 20 μm (Goueffon et al., 2010a). In this study, the electrolyte concentration (C) and the anodizing temperature (T) were adjusted to control the film's initial porosities. Thus, two types of selected and prepared anodic films are 40% (C_1 = 150 g/L; T_1 = 20 °C) and 50% (C_1 = 150 g/L; T_1 = 25 °C) of porosities.

The anodized parts were then coloured by successive immersions in two different baths. Firstly a solution of cobalt acetate (200 g/L) at 43 °C was used to fill in the pores during 15 min. Secondly, an immersion in ammonium sulphide (30 g/L) at room temperature during 10 min resulted in the precipitation of black dyes (CoS) in the pores.

The final step was a sealing in an aqueous solution of nickel acetate (5 g/L) and boric acid (5 g/L) at 98 ± 2 °C. The hydration of the oxide was used to close pores and protect dyes.

A previous study (Goueffon et al., 2009b) showed that films with initial porosities of 40% and 50% were crazed after colouring and sealing steps. Actually, the differential thermal dilatations in the sealing bath, associated to a poor limit tensile stress of highly porous films, were proved to lead to formation of cracks perpendicular to the interface during the process. In both cases residual stresses from the process were relaxed by the crazing.

2.2. Ageing

To simulate the space environment, the ESA Standard (ECSS-Q-ST-70-04C, 2008) recommends performing 100 cycles between −100 and +100 °C under vacuum (10^{-5} Pa) with a dwell time of at least 5 min and a slope of 10 °C per minute. These conditions were defined for the general case and all kinds of materials (from polymers to metals). The number cycles' impact, the pressure and the temperature range on the adhesion will be evaluated in this paper. A Sun Electronic System EC11 environmental chamber was used to perform thermal cycles. Dwells times of 5 min and warming/cooling speeds of 10 °C/min under nitrogenous atmosphere were used. Nevertheless, this speed was 1 °C/min for cycles performed under vacuum (10^{-6} Pa) because of the warming system.

2.3. Adhesion measurements

2.3.1. Peel tests

Adhesion was evaluated qualitatively using 90° peel tests with tape strengths of 250 and 670 g/cm. The removal speed was 500 mm/min controlled with tensile testing device (Instron). Three identical samples were tested for each configuration with each tape to observe an average behaviour.

2.3.2. Scratch test

The adhesion was quantitatively evaluated using a scratch-test device (CSM Revetest instrument) with a diamond stylus (Rockwell, 200 μm radius tip). Scratch tests were configured with an increasing normal load from 1 to 60 N, a loading speed of 30 N/min and an advance speed of 5 mm/min. The mechanism of degradation was the lateral flaking of the film on both sides of the scratch (Bull, 1997). The resulting scratch-print of about 10 mm length was then observed by Scanning Electron Microscopy (SEM – Philips XL30 ESEM) to determine the corresponding normal load. The given values are averages of six different scratches on each sample.

2.3.3. Four-point bending test

Four-point bending tests with acoustic emission were also performed to evaluate the evolution of adhesion of the film (Delmas et al., 2001; Ollendorf and Schneider, 1999; Richard et al., 1996). Tests were done on a tensile testing device (Adamel DY 26 of 100kN) with a distance between supports of 40 mm for the face under compression

and 120 mm for the face under tension. Samples ($10 \times 20 \times 160$ mm) were anodized and black coloured only on the compressive face between the supports. All the anodic film is then submitted to a uniform strain field. The tests were coupled with acoustic emission measurements to determine the damaging loads. The detection threshold was set at 50 dB to filter noise. In this configuration, no acoustic hit is detected during the bending of an unanodized aluminium sheet. Samples were observed by SEM after loading to determine if flaking occurred. Three samples were tested to obtain an average value of bending critical load.

2.4. Evaluation of the dehydration

Thermo-gravimetric analysis (TGA) were carried out to evaluate the kinetic of water desorption during thermal cycles. The anodic film was isolated from the substrate by mechanical compression. Actually, samples were four-point bent until delaminating of the anodic film on the compressive face. The film was thus collected under powder form. A speed of 10 °C/min, dwells times of 5 min, and a nitrogenous atmosphere were used. A test at constant temperature under a pressure of 10^2 Pa was also performed. All measurements were realised with a Setaram B24 thermo-balance.

2.5. Numerical simulation

As the anodic films elaborated at 20 and 25 °C (40% and 50% initial porosity) are crazed after the whole black anodizing process (Goueffon et al., 2009b), a finite element simulation was used to evaluate mechanical behaviour of a crazed thin film on its substrate during thermal cycling. The software SAMCEF was used to perform isotropic thermo-elastic calculations with 2-dimensional plane strain hypotheses. The geometry used was a substrate (thickness of 3 mm) with an anodic film of 20 μm thick. Mechanical characteristics of the substrate used for the calculations can be found in the literature (Davis, 1993) and were the following: Young modulus of 72 GPa, Poisson's ratio of 0.33 and Coefficient of Thermal Expansion (CTE) of $23.6 \times 10^{-6}\,K^{-1}$. Concerning the film, previous studies (Goueffon et al., 2010a) proved that the Young modulus is linked to the porosity and those different values were used. Poisson's ratio was chosen to 0.28 (Goueffon et al., 2010b) and the CTE value ($13 \times 10^{-6}\,K^{-1}$) was previously obtained by beam bending analysis (Goueffon et al., 2010b). Cracks with various geometries (1 micron width and variable length) were added through the film. Boundary conditions were defined in order to permit free deformations of the system under thermal loadings. Applied loadings were only thermal, constant and uniform. The temperature was chosen between −140 and +140 °C while the reference of the system is 20 °C. All stresses in the model are then due to differential thermal dilatations between the film and the substrate. A contact criterion has been implemented between the two lips of the crack. The friction coefficient was set up at 0.3. A study on the sensibility of this parameter in the range from 0.1 to 0.5 has shown that its influence on the calculated stress intensity factors is negligible.

Meshing of the whole model and of the crack tip has been validated by comparing the stress intensity factor K_I in the case of a straight crack perpendicular to the surface with theoretical values (Anderson, 2005) on a mono-material (same mechanical properties for substrate and film) and with numerical values for a bi-material (Kaddouri et al., 2006) at room temperature.

Thus, the potential evolution of a crack through the coating was evaluated when thermally loaded by considering the stress intensity factors. These stress intensity factors were calculated thanks to the Equivalent Domain Integral (EDI) Method (Bittencourt et al., 1996) and strain energy density criterion was used to evaluate the bifurcation angle of the crack (Sih, 1973). The crack will propagate if $K > K_C$ (Irwin, 1956) where K_C is the toughness of the film. However, in the present study, toughness of the anodic film has not been determined. Consequently, results from the numerical simulation are not able to quantitatively predict conditions of cracking. Nevertheless, comparative analyses of the K values can give information on the cases that are potentially the more detrimental and that can favour crack propagation.

3. Experimental results and discussion

3.1. Influence of the pressure on the adhesion of the film

Both types of black anodic films (40% and 50% of initial porosities) were cycled ten times between −80 and +80 °C. The influence of the atmosphere (inert gas or vacuum) used during thermal cycling on the adhesion of anodic films was particularly studied.

The evolution of the scratch-test critical load was observed after thermal cycling (Fig. 1). After cycles under nitrogenous atmosphere, the measured critical load is affected only for the anodic films with the highest initial porosity (from 20 N to 5 N). However, cycles performed under vacuum are detrimental for both types of films, with the same effect than inert gas for film with 50% of initial porosity while a slight decrease of the scratch critical load of the film with 40% of porosity is observed.

Four-point bending tests were also realised after the same ageing. Before thermal cycling, no acoustic signal is

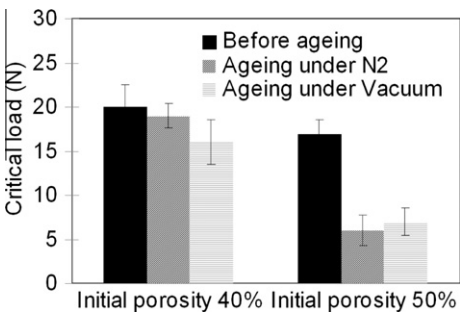

Fig. 1. Evolution of the scratch critical load measured after 10 thermal cycles between −80 and +80 °C under N_2 or vacuum (10^{-6} Pa) for samples with two different initial porosities (40% and 50%).

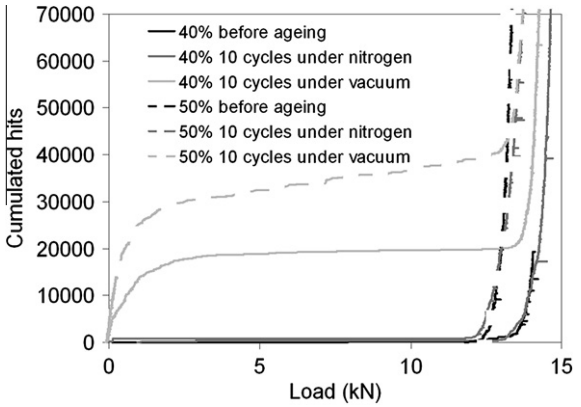

Fig. 2. Cumulated hits detected by acoustic emission measurements as a function of the load of four-point bending: samples with 40% and 50% of initial porosity and different ageing.

detected before a critical load which depends on the porosity of the film (Fig. 2). The bending critical load corresponds to plastic strains of the aluminium substrate. Those acoustic hits are here associated to the degradation of the film under compressive stresses. After thermal ageing under vacuum, both types of samples have a modified behaviour during bending. Acoustic events are detected at low loads: they can be attributed to propagations of cracks created during the sealing step in the anodic film. After thermal ageing under nitrogenous atmosphere, very few acoustic hits are detected at low loads in the case of samples with a porosity of 50%. No acoustic event is detected for the samples with a porosity of 40%.

Those results are consistent with peel tests. Before or after thermal ageing under nitrogen of samples with 40% of porosity, no particle of the coating is detached from the substrate, whatever the tape used. After cycles under vacuum, the tape test results in several particles removed with the 250 g/cm tape while numerous are detached with the 670 g/cm one (Fig. 3). For samples with 50% of porosity, cycles under inert gas or vacuum are both leading to flaking.

The decrease of the critical load in scratch-test, bending-test or peel-test after thermal cycling is attributed to

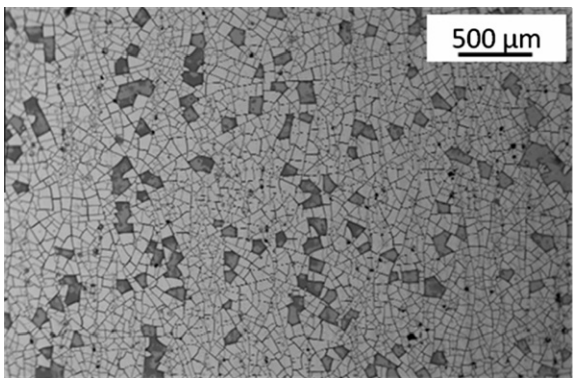

Fig. 3. Surface SEM observation of an anodic film (initial porosity 40%) after 10 thermal cycles under vacuum between −80 and +80 °C and peel test (670 g/cm).

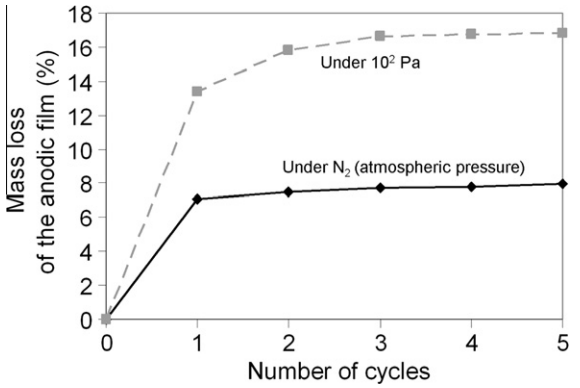

Fig. 4. Thermo-gravimetric analysis of anodic films with initial porosity of 40% during cyclic warming at +80 °C.

crack propagations in the film during ageing. Actually, during thermal cycling, the differential thermal dilatations between the film and the substrate results in tensile stresses in the film during heating and compressive stresses for temperatures lower than the ambient. These stresses can cause crack propagation. However, as observed for films with 40% of initial porosity, temperature range is not the only parameter affecting the adhesion: temperatures between −80 and +80 °C under inert gas are not modifying the adhesion. Nevertheless, thermal cycling at the same temperatures under vacuum has a detrimental effect on the adhesion.

Fig. 4 shows the mass loss of an anodic film during the thermal cycles between −80 and +80 °C under a nitrogen flux at ambient pressure and under a low pressure (10^2 Pa). The mass loss is more important at low pressure than with an inert gas. Those observations are even confirmed at ambient temperature (Fig. 5). So the dehydration of black anodic films occurring during thermal cycles is amplified by the vacuum. This phenomenon results in additional tensile stresses in the film (Goueffon et al., 2009b) favourable to cracks development. After several days in a vacuum of 10^{-6} Pa at ambient temperature, the cracks width increases (Fig. 6) what is a consequence of the dehydration (Rayhani et al., 2008). Nevertheless, seven days in a vacuum atmosphere without thermal stresses have no influence on any adhesion measurement

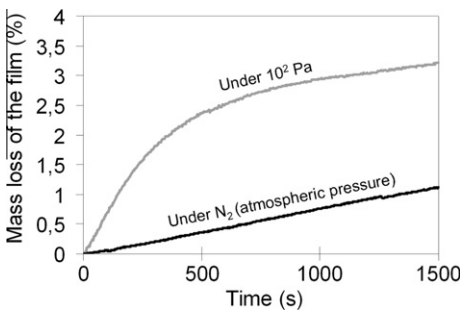

Fig. 5. Thermo-gravimetric analysis of anodic films with initial porosity of 40% at ambient temperature.

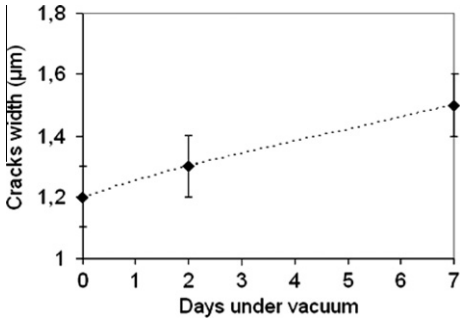

Fig. 6. Evolution of the cracks width on a 40% porosity film as a function of the time of storage under vacuum (10^{-6} Pa) at ambient temperature.

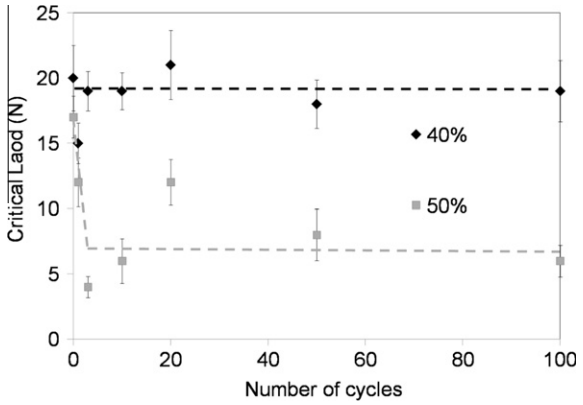

Fig. 7. Evolution of the scratch-test critical load as a function of the number of thermal cycles between −80 and +80 °C under nitrogenous atmosphere.

performed. Thus, the loss of adhesion during thermal cycling is a consequence of combined thermal and dehydration stresses.

3.2. Influence of the number of cycles on the adhesion

Fig. 7 presents the evolution of the scratch critical load as a function of the number of thermal cycles performed between −80 and +80 °C under nitrogenous atmosphere. Films with an initial porosity of 40% are not damaged even for a high number of thermal cycles. This result was confirmed by four-point bending tests and peel tests. Actually, when degradation occurs, it is during the first thermal cycles as we can see for the sample showing initial 50% porosity. This observation is confirmed under vacuum for both types of porosities (Fig. 8).

These results must be related with the fast dehydration that mainly occurs during the first cycles, as seen in Fig. 4. In addition, they are consistent with the brittleness of the anodic film: the mechanism of degradation is not cyclic loading but results from the combined effect of thermal and dehydration stresses that damage the film quasi-immediately.

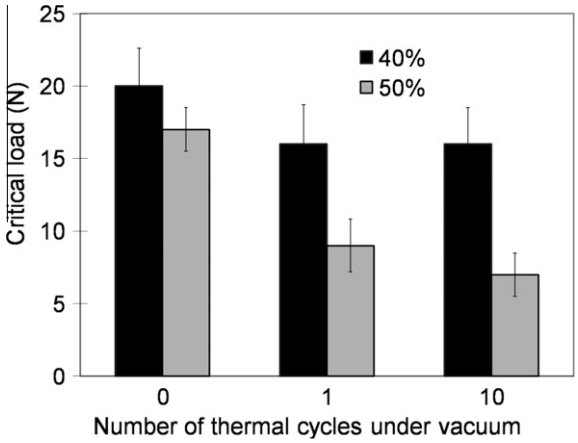

Fig. 8. Evolution of the scratch-test critical load as a function of the number of thermal cycles between −80 and +80 °C under vacuum (10^{-6} Pa).

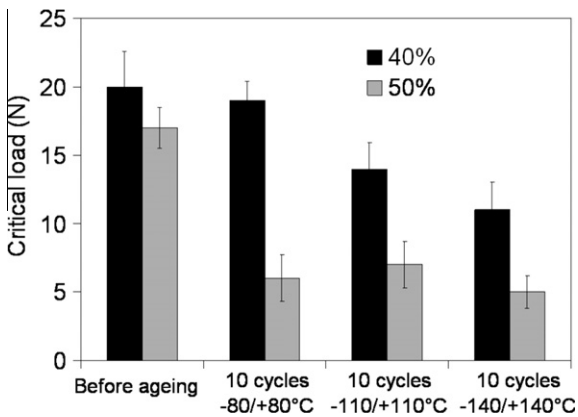

Fig. 9. Evolution of the scratch-test critical load as a function of the temperature of thermal cycles under nitrogenous atmosphere.

3.3. Effects of the temperature range

The influence of temperature range has been investigated for both types of anodic films after ten thermal cycles under nitrogen atmosphere (Fig. 9). The adhesion of anodic films with an initial porosity of 50% was already degraded with thermal cycles between −80 and +80 °C. The scratch-test critical load measured after ageing was around 5 N. Ageing with larger temperature range is also leading to the same results (Fig. 9). Nevertheless, if samples with a lower initial porosity (40%) are not affected by thermal cycles −80/+80 °C, the increase of the temperature range (−110/+110 °C and −140/+140 °C) is leading to a progressive decrease of the critical load.

For all types of samples four-point bending is not leading to significant results. This can be attributed to the fact that the dehydration is not complete at 140 °C at ambient pressure under nitrogenous atmosphere. After thermal cycling under nitrogen, any eventual fracture in the hydrated anodic film with 50% of initial porosity during

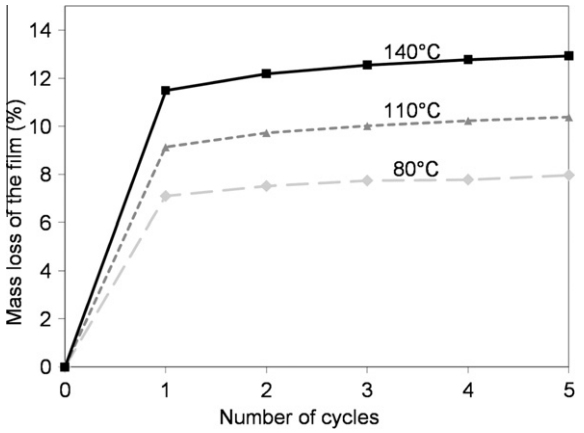

Fig. 10. Thermo-gravimetric analysis of anodic films with initial porosity of 40% under inert atmosphere for different temperatures of cycling.

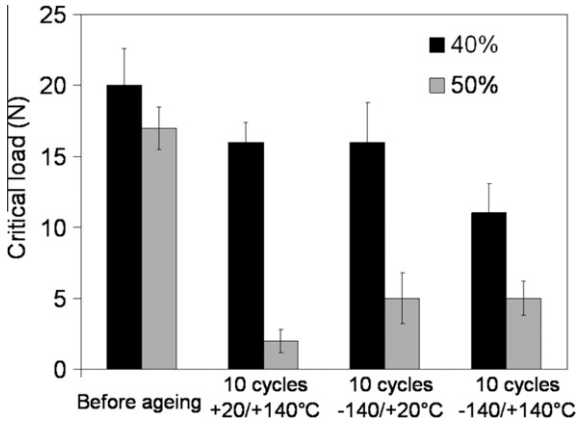

Fig. 11. Evolution of the scratch-test critical load with dissociating cold parts and hot parts of thermal cycles (−140/+140 °C) under nitrogenous atmosphere.

four-point bending could lead to acoustic emission with amplitudes lower than the detection threshold (50 dB).

For 50% of initial porosity, peel-tests are always leading to particles detachment after ageing, whatever the temperature of cycling. Films with the lower porosity are not damaged by peeling during cycling between −80 and +80 °C. For the two larger temperature ranges tested, some particles are pulled up with both tapes used.

The detrimental influence of increasing temperature range is due to two phenomena. Firstly, the increase of the temperature range is resulting in higher thermal stresses in the anodic films because the stresses induced by differential dilatations are proportional to the temperature (Goueffon et al., 2009b). Secondly, the dehydration and then associated tensile stresses in the film are amplified when the maximum temperature reached increases (Fig. 10). The cracks are then more solicited and may propagate in the film.

To understand the mechanisms leading to the collapse of adhesion during ageing, it is now necessary to dissociate the influence of the cold temperatures (<20 °C) and hot ones (>20 °C) during cycling.

3.4. Dissociation cold/hot parts of thermal cycles

The contributions of each part of the thermal cycling to the loss of adhesion were studied for 10 cycles between −140 °C and +140 °C under nitrogen. During cycling between −140 and 20 °C, no dehydration may occur (Fig. 11). The film is then only solicited with compressive stresses due to differential dilatations. On the contrary, between 20 and 140 °C, the dehydration and then tensile stresses in the film may be equivalent than during cycles between −140 and 140 °C. Fig. 11 shows that the decrease of critical load for samples with an initial porosity of 40% is less important for cycles with amplitudes of 20/140 °C or −140/20 °C than for −140/+140 °C.

Tensile and compressive stresses level reached during cycling are separately responsible of a small loss of adhesion of the film. However, successions of hot and cold loadings are more damaging for black anodic films.

3.5. Influence of the initial porosity of the anodic film

As seen on all the results presented in the previous sections, the loss of adhesion due to ageing is different for the films with 40% and 50% of initial porosity. In particular, some ageing conditions can seriously affect the adhesion of the film with the highest porosity while they do not modify the behaviour of the film showing 40% initial porosity. In addition when they are both affected for a given ageing condition, the loss of adhesion (see quantitative results obtained by scratch tests), is more important for high porosity films. Thus, films with 50% of initial porosity seem to be more sensitive to thermal ageing. The difference of anodizing temperature between films with 40% and 50% porosity is only 5 °C. So an insufficient control of the bath temperature could explain the apparent non reproducibility of measurements performed after ageing classically encountered on black anodic films.

3.6. Analysis of the flaking

The black anodic films were observed by SEM after ageing and adhesion evaluation. These observations were performed after four-point bending, scratch test and peel test, especially where particles were pulled-off (Fig. 12). The sulphur detected by additional energy-dispersive X-ray spectroscopy (EDX) analyses, performed at the bottom of the print let by the particle, have shown that the fracture is cohesive in the film. Thus, the cracks propagate only in the film and then bifurcate before the interface film/substrate as schematically presented Fig. 13.

A finite element model was developed to better understand the types of solicitations leading to these crack bifurcation and propagation along the interface.

4. Numerical results and discussion

4.1. Crack propagation through the thickness of the film

The stress state near the crack when the sample is thermally loaded was evaluated thanks to the finite element

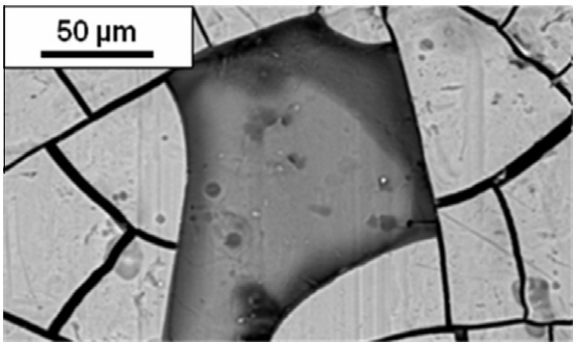

Fig. 12. Surface SEM observation of black anodic film (initial porosity 50%) after 10 cycles between −80 and +80 °C and peel test with a tape strength of 250 g/cm.

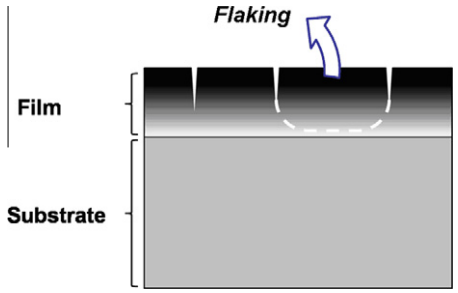

Fig. 13. Schema of crack propagation in an anodic film leading to flaking.

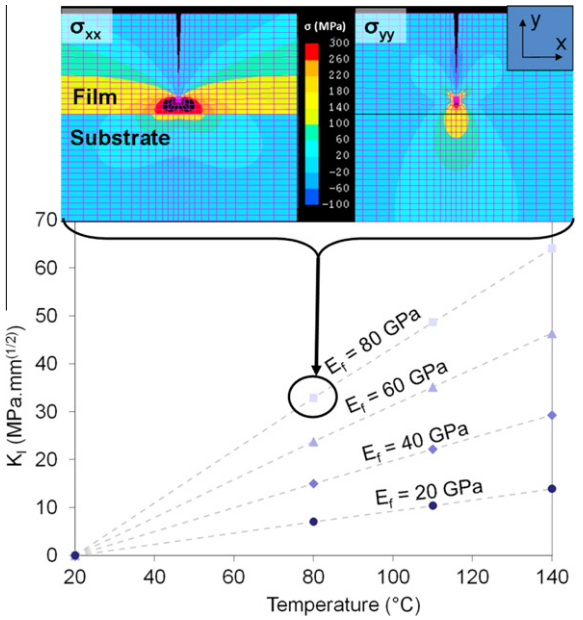

Fig. 14. Evolution of the stress intensity factor K_I of a 17 µm length crack as a function of the applied temperature and for different Young modulus of the film. The stress state around a crack tip is presented on the upper part of the figure.

model. Effects of dehydration are not modelled here, only thermal stresses due to the dilatations mismatch are calculated. At 80 °C, thermal tensile stresses are released on both sides of the crack; nevertheless a stress concentration is observed near the tip (Fig. 14). The Young modulus of the film decreases when its initial porosity increases (Goueffon et al., 2010a). It can vary from approximately 90 GPa (10% of initial porosity) to less than 20 GPa (50% of initial porosity). Thus, the stress intensity factors were calculated for different young modulus of the film as a function of the temperature applied (Fig. 14). Whatever the modulus of the film considered, the crack is only solicited in mode I (K_{II} = 0 MPa $m^{1/2}$). When the temperature is lower than 20 °C, the film is under compressive thermal stresses, thus the crack is closed and the tip is not solicited. For higher temperatures, the stress intensity factor corresponding to the opening mode K_I is linearly increasing with the temperature as expected. For a given temperature and a given crack length, stress intensity factor increases when Young modulus of the film increases: the crack propagation will be favored in films of higher Young modulus.

4.2. Bifurcation of the crack

In the previous conditions, there is symmetry of the geometry and loadings: the propagation angle is always equal to zero. It is necessary to break this symmetry to cause the bifurcation of the crack. The first possibility is the initial deviation of the crack. Actually, on experimental samples, cracks are not always exactly perpendicular to the interface. It can be explained by the roughness of the film ($Ra \approx 1.6$ µm) and the presence of defects at its surface (Goueffon et al., 2009a). The crack was then designed with an initial angle ψ which can vary between 0° and 10° (Fig. 15).

At −80 or 120 °C, K_I is not significantly modified by the presence of a small initial angle (Fig. 16). Nevertheless, we can observe in both cases the apparition of K_{II} (shearing mode) when ψ increases.

At hot temperatures, the crack is then under a mixed mode (I + II) but $K_I >> K_{II}$ then it can be assimilated as pure mode I. The bifurcation angle is then tending to redress the crack perpendicularly to the interface (Fig. 16). At cold temperatures the solicitations are purely in the mode II resulting in a bifurcation angle of approximately 70°. Nevertheless, the value of K_{II} is low ($K_{II}^{120°C} < K_{II}^{-80°C} << K_I^{120°C}$), so the temperature has to be cold enough to generate crack propagation.

A second possibility to break the symmetry is to insert neighbour cracks in the model (Fig. 17). Two cracks (17 µm length) were added to the initial model at a distance of 100 µm on both sides of the first one. This corresponds to the average size of islets observed on samples with scanning electron microscopy (Fig. 3). The central crack was then moved off centre at a distance "*e*". When *e* increases, the central crack closers to its neighbour and enters in its stress field. The symmetry of the stress field is then broken resulting in the simultaneous apparition of a mode II and release of the mode I. This phenomenon is amplified when the cracks become closer (i.e. when *e* increases) (Fig. 18).

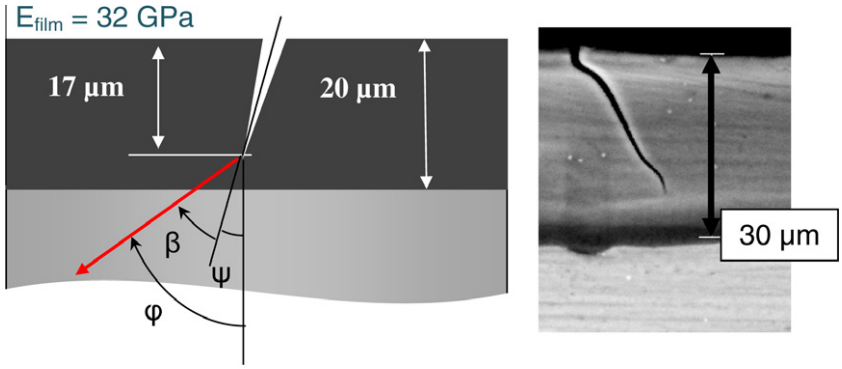

Fig. 15. Schema of the crack geometry with an initial angle (on the left) and comparison with SEM cross-section view (on the right).

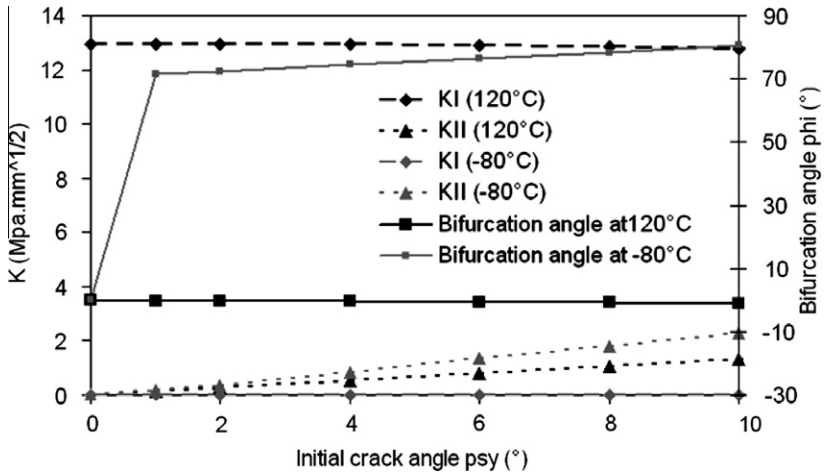

Fig. 16. Evolution of the stress intensity factors and the bifurcation angle for an initial angle from 0° to 10° (E_f = 32 GPa).

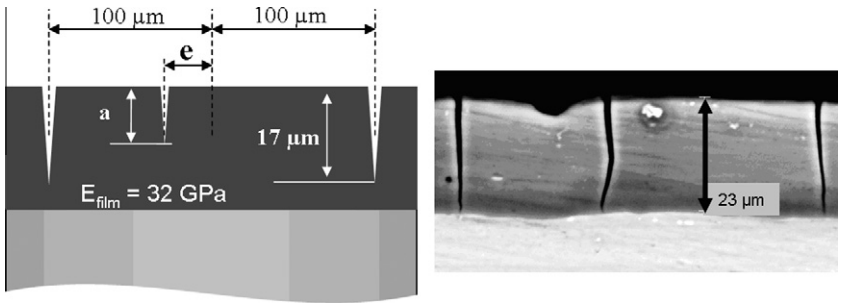

Fig. 17. Schema of the film with three cracks (on the left) and comparison with SEM cross-section view (on the right).

The apparition of this mixed mode is generating a crack bifurcation. The corresponding angle is actually increasing with e but is somewhat dependant on the central crack length (Fig. 18).

Two major causes of crack bifurcation have been highlighted. First, a geometrical asymmetry can lead to a pure mode II loading of the crack at temperatures lower than 20 °C. The temperature has to be cold enough to generate the propagation of the crack with a bifurcation angle of approximately 70°. Secondly, a close crack (or local defect) unbalances the stress field around the crack which is then solicited in mixed mode (I + II). The bifurcation angle is then strongly depending on the ratio K_I/K_{II} and thus on the distance to the neighbour crack.

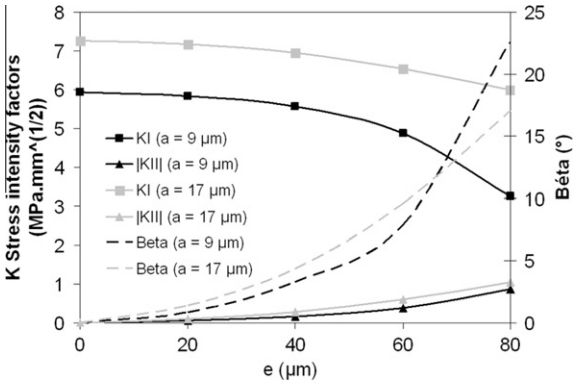

Fig. 18. Stress intensity factors and bifurcation angle of the central crack as a function of its eccentricity (a = 9 µm or a = 17 µm, T = 120 °C and E_{film} = 32 GPa).

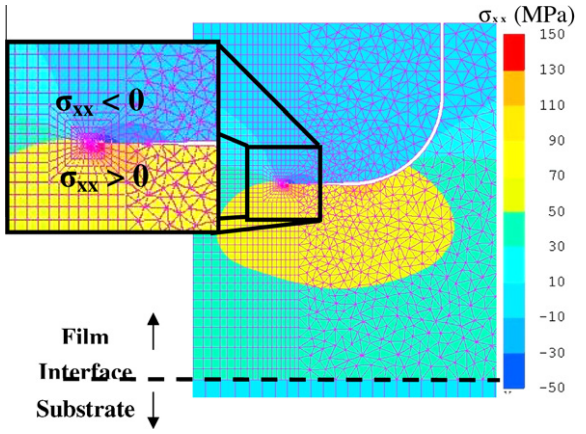

Fig. 20. Stress field (σ_{xx}) around the crack tip at 80 °C (r = 5 µm, W = 10 µm, a = 9 µm, E_{film} = 32 GPa).

4.3. Propagation along the interface film/substrate

The shape of the initial model has been modified to study the crack propagation along the interface. A kinked crack was designed with depth "a", a global width "W" and a radius of curvature "r" (Fig. 19).

At 80 °C, the substrate strains generate tensile stresses in the film. Stress concentration between the crack and the interface is observed. However, strains are not transmitted to the upper part of the film. A released area and even local compressive stresses near the crack tip appear (Fig. 20), creating local shear loading (mode II).

At hot temperatures (T > 20 °C), Fig. 21 shows that the crack is also solicited in opening mode (mode I). At cold temperatures (T < 20 °C), K_I = 0 MPa m$^{1/2}$, thus the crack is solicited in pure mode II. In both cases, the intensity of the solicitations is proportional to the applied temperature.

It is worthwhile to notice that the choice of the radius r does not have any significant effect on the values of calculated stress intensity factors. However, when the crack depth increases, these factors (mode I and II) are more important (Fig. 22).

Thus, the propagation along the interface will be favoured if the initial crack is deep enough.

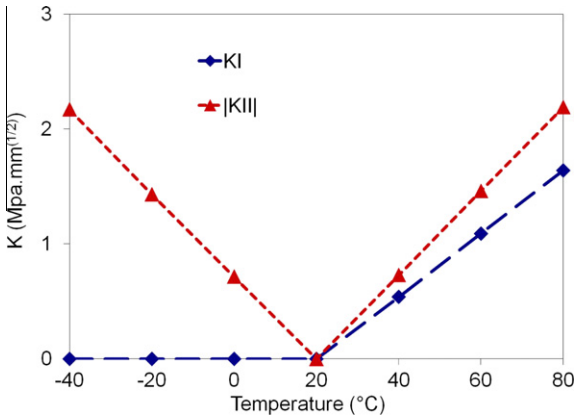

Fig. 21. Stress intensity factors as a function of the thermal loading applied (r = 5 µm, W = 10 µm, a = 9 µm, E_{film} = 32 GPa).

5. Global discussion on the degradation mechanisms of black anodic films

The decrease of adhesion detected on several black anodic films after ageing was attributed to the propagation of

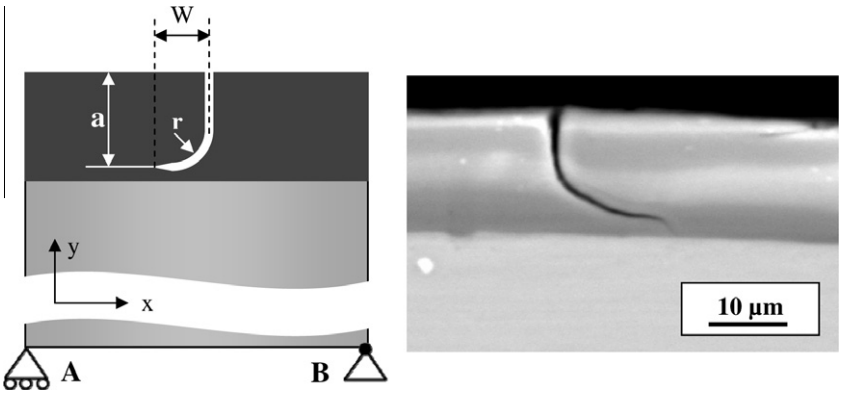

Fig. 19. Schema of the numerical model with a kinked crack (on the left) and comparison with SEM cross-section view (on the right).

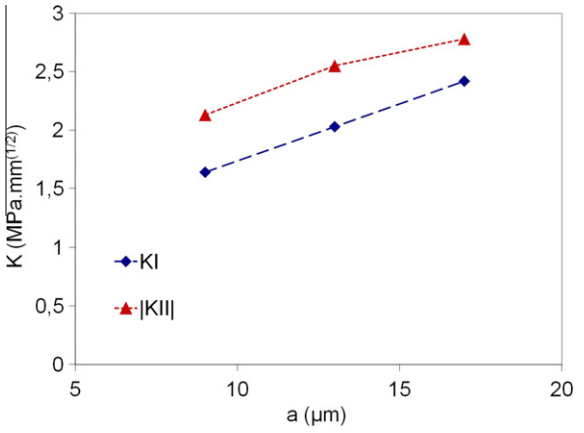

Fig. 22. Stress intensity factors at 80 °C for different crack depths (r = 5 μm, W = 10 μm, E_{film} = 32 GPa).

cracks initiated during the process. Adhesion measurements have shown an important difference of behaviour between films with 40% and 50% of initial porosities. Flaking occurs much easier on films with the highest initial porosity.

Yet, the Young modulus of these highly porous films is lower than for other films (Goueffon et al., 2010a). According to the Fig. 14, the stress intensity factors are then lower in films at 50% of initial porosity than in 40% initial porosity films at a given temperature. The difference between the two samples can then be explained by two hypotheses. Firstly, it can be attributed to the fact that cracks resulting from the colouring and sealing processes are thicker and then probably deeper in the highest porosity film as noted in Goueffon et al. (2010a) and Liu et al. (2008). So, according to numerical results (Fig. 22), this could result in slightly higher values of stress intensity factors for the 50% of initial porosity films. Secondly, and with probably a more important influence, this could be due to a decrease of the toughness K_c with the increasing porosity as Hashimoto et al. (2007) have observed on ceramics.

With these hypothesis, stresses (thermal + dehydration) encountered during thermal cycling between −80 and +80 °C are not high enough to cause crack propagation in films with 40% of initial porosity. The toughness of the films with 50% of initial porosity being lower, crack propagation can occur resulting in the loss of adhesion detected by peel-tests and scratch-tests.

The thermal cycling range enlargement implies an increase of stress intensity factors as noted by numerical analysis (see for instance Fig. 14). Crack propagation occurs between −110 and +110 °C (and then −140/+140 °C) for films with 40% of initial porosity and an adhesion loss is detected. The vacuum amplifies tensile stresses in the films, especially at hot temperatures. Actually, the release of water favours crack propagation what explains the lower critical loads measured by scratch-tests after ageing under vacuum than under nitrogenous atmosphere.

The numerical model has shown that a bifurcation of the crack can be induced by the presence of a neighbour crack, a defect, or cold temperatures. The crack can then propagate along the interface either under mixed mode I + II at hot temperatures or under pure mode II at cold temperatures, justifying the respective detrimental effect of only cold temperatures cycling and only hot temperatures cycling on the adhesion, as noted experimentally (Fig. 11).

6. Conclusion

On the three methods used to evaluate the adhesion of black anodic films on their substrates, two of them (scratch test and peel test) have clearly spotted an ageing effect during thermal cycling. A flaking of the film can occur and the associated fracture is cohesive in the film. Numerical simulation has shown that thermo-mechanical solicitations (differential dilatations) related to both warm and cold parts of the thermal cycling can cause crack propagations according to different mechanisms, what could result in a loss of the measured adhesion. Samples with the highest initial porosity are the more sensitive to flaking. It can be explained by their low toughness favoring crack propagation.

When this adhesion loss occurs, it is detected after the first thermal cycles. The fast propagation is consistent with the brittle behaviour and the instable character of crack propagation. The loss is more important in vacuum due to additional effects of dehydration. When the range of thermal cycles increases, the stresses, due to differential dilatations or dehydration, are amplified arising risks of crack propagations.

Acknowledgements

The authors thank Rafal Pijewski and Muguette Monjauze for their participations to this study.

References

Agrawal, B.N., 1986. Design of Geosynchronous Spacecraft. Prentice-Hall, Englewood Cliffs, NJ, USA.

Anderson, T.L., 2005. Fracture Mechanics: Fundamentals and Applications, third ed. Taylor & Francis, Boca Raton, USA, pp. 43–44.

Bittencourt, T.N., Wawrzynek, P.A., Ingraffea, A.R., Sousa, J.L.A., 1996. Quasi-automatic simulation of crack propagation for 2D LEFM problems. Eng. Fract. Mech. 55, 321–334.

Bull, S.J., 1997. Failure mode maps in the thin film scratch adhesion test. Tribol. Int. 30, 491–498.

Davis, J.R., 1993. ASM Specialty Handbook: Aluminum and Aluminum Alloys. ASM International, Materials Park, OH, USA, pp. 73–75.

Delmas, D., Benmedakhene, S., Richard, C., Abdelouahed, L., Béranger, G., Grégoire, T., 2001. Characterization of adherence and cracking within coated materials by an acoustic emission method: application to a WC-Co coating on a steel substrate. Surf. Chem. Catal. 4, 345–350.

ECSS-Q-ST-70-03C, 2008. ESA Standard, Black-Anodizing of Metals with Inorganic Dyes. <http://www.ecss.nl>.

ECSS-Q-ST-70-04C, 2008. ESA Standard, Thermal Cycling Test for the Screening of Space Materials and Processes. <http://www.ecss.nl>.

ESA Alert, 2005, EA-2005-MEP-02-B. PSS-01-703 Inadequate for 2XXX and 7XXX Alloys. Available at: <http://alerts.esa.int/>.

Goueffon, Y., Arurault, L., Mabru, C., Tonon, C., Guigue, P., 2009a. Black anodic coatings for space applications: study of the process parameters, characteristics and mechanical properties. J. Mater. Process. Technol. 209, 5145–5151.

Goueffon, Y., Mabru, C., Labarrère, M., Arurault, L., Tonon, C., Guigue, P., 2009b. Mechanical behaviour of black anodic films on 7175 aluminium alloy for space applications. Surf. Coat. Technol. 204, 1013–1017.

Goueffon, Y., Arurault, L., Fontorbes, S., Mabru, C., Tonon, C., Guigue, P., 2010a. Chemical characteristics, mechanical and thermo-optical properties of black anodic films prepared on 7175 aluminium alloy for space applications. Mater. Chem. Phys. 120, 636–642.

Goueffon, Y., Mabru, C., Labarrère, M., Arurault, L., Tonon, C., Guigue, P., 2010b. Investigations into the coefficient of thermal expansion of porous films prepared on AA7175 T7351 by anodizing in sulphuric acid electrolyte. Surf. Coat. Technol 205, 2643–2648.

Hashimoto, R., Murakami, A., Miyata, H., Katagari, K., 2007. Effect of Dy211 content on fracture toughness of Dy123 bulks. Physica C 463, 357–361.

Irwin, G., 1956. Analysis of stresses and strains near the end of a crack traversing a plate. J. Appl. Mech. 24, 361–364.

Kaddouri, K., Belhouari, M., Bachir Bouiadjra, B., Serier, B., 2006. Finite element analysis of crack perpendicular to bi-material interface: case of couple ceramic–metal. Comput. Mater. Sci. 35, 53–60.

LeVesque, R., Ho, M., Vickers, B., Babel, H., Pard, A., 1992. Black anodize as a thermal control coating for space station freedom. AIAA-92-2160-CP. In: AIIA Technical Papers (A92-31285 12-23), Washington, USA, pp. 56–65.

Liu, W., Zuo, Y., Tang, Y., Zhao, X., 2008. The cracking behavior of anodic films on cast aluminum alloy after heating in the temperature range up to 300 °C. Surf. Coat. Technol. 202, 4183–4188.

Magdy, A., Ibrahim, M., 2006. Black nickel electrodeposition from a modified Watts bath. J. Appl. Electrochem. 36, 295–301.

McCroskey, D.M., Abell, G.C., Chidester, M.H., 2000. Aeroglaze Z306 black paint for cryogenic telescope use: outgassing and water vapor regain. In: SPIE the International Society for Optical Engineering, Proceeding SPIE, vol. 4096, pp. 119–128.

Ollendorf, H., Schneider, D., 1999. A comparative study of adhesion test methods for hard coatings. Surf. Coat. Technol. 113, 86–102.

Rayhani, M.H.T., Yanful, E.K., Fakher, A., 2008. Physical modeling of desiccation cracking in plastic soils. Eng. Geol. 97, 25–31.

Richard, C.S., Béranger, G., Lu, J., Flavenot, J.F., Grégoire, T., 1996. Four-point bending tests of thermally produced WC-Co coatings. Surf. Coat. Technol. 78, 284–294.

Saxena, V., Uma Rani, R., Sharma, A.K., 2006. Studies on ultra high solar absorber black electroless nickel coatings on aluminum alloys for space application. Surf. Coat. Technol. 201, 855–862.

Shashikala, A.R., Sharma, A.K., Bhandari, D.R., 2006. Solar selective black nickel–cobalt coatings on aluminum alloys. Sol. Energ. Mater. Sol. Cells 91, 629–635.

Shrestha, S., Shashkov, P., Dunn, B.D., 2006. Microstructural and thermo-optical properties of black Keronite PEO coating on aluminium alloy AA7075 for spacecraft materials applications. In: Proceedings of ISMSE & ICPMSE, SP-616. ESA Publication Division, Collioure, France, pp. s1.5.1–s1.5.9.

Sih, G.C., 1973. Some basic problems in fracture mechanics and new concepts. Eng. Fract. Mech. 5, 365–377.

Siva Kumar, C., Mayanna, S.M., Mahendra, K.N., Sharma, A.K., Uma Rani, R., 1999. Studies on white anodizing on aluminium alloy for space applications. Appl. Surf. Sci. 151, 280–286.

Wu, X., Qin, W., Cui, B., Jiang, Z., Guo, Y., Xie, Z., 2007. The influence of the time on the optical properties of the ceramic thermal control coating prepared by micro-plasma oxidation. J. Mater. Sci. 42, 7251–7255.